STRUCTURE, PHASE TRANSFORMATIONS, AND DIFFUSION

Microstructure of a Laser-Welded Joint between a Chromium–Nickel Steel and a Titanium Alloy with a Copper Insert

N. B. Pugacheva[a], *, E. I. Senaeva[a, c], E. G. Volkova[b], A. V. Makarov[a, b, c], and L. S. Goruleva[a]

[a]*Institute of Engineering Science, Ural Branch, Russian Academy of Sciences, Ekaterinburg, 620049 Russia*
[b]*Mikheev Institute of Metal Physics, Ural Branch, Russian Academy of Sciences, Ekaterinburg, 620990 Russia*
[c]*Ural Federal University n.a. the First President of Russia B.N. Yeltsin, Ekaterinburg, 620002 Russia*
*e-mail: nat@imach.uran.ru

Abstract—The microstructure of a laser-welded joint between a chromium–nickel austenitic steel and a titanium alloy with an intermediate copper insert has been studied. Using X-ray diffraction analysis, energy-dispersive X-ray microanalysis, and transmission electron microscopy, it has been shown that the welded joint represents a copper-based solid solution with intermetallic particles of $(Fe,Cr)_2Ti$ and Cu_3Ti 10–50 μm in size, which were the first to crystallize in the welding pool, and intermetallic particles of $(Fe,Cr)_2Ti$ and Cu_4Ti with a size of no more than 30 nm, which homogeneously precipitate on cooling from the copper-based solid solution oversaturated at the moment of crystallization. The fracture of the joint upon tensile tests occurred along the diffusion zone at the boundary with the titanium alloy. The maximum ultimate tensile strength of such a joint was 474 MPa.

INTRODUCTION

The desire to reduce the weight of modern high-speed vehicles (cars, boats, rail and air transport) envisages a task to join dissimilar materials, for example, steel with aluminum or titanium alloys [1]. The main problems of welding unlike materials are their different thermophysical properties (melting point, heat capacity, thermal conductivity, and thermal expansion coefficient) and limited solubility of one metal in another because of the differences in their crystal structure [2–4]. In the course of crystallization of the melt in the welding pool upon the welding of a steel with a titanium alloy, intermetallic particles Fe_2Ti and $FeTi$ are formed, which produce a continuous interlayer in the material of the welding joint (WJ). This can lead to the appearance of a through crack after cooling and to the violation of the continuity of the joint [3, 5, 6]. To form solid solutions in the WJs of chromium–nickel steels with titanium alloys, intermediate inserts are successfully used. These inserts should satisfy the following requirements [7–10]: (1) their thermophysical properties should be close to the corresponding properties of the joined materials; (2) the crystal lattices of the inserts should be maximally conjugated with those of the joined metals; (3) the melting point of the insert should be lower than that of the joined metals; (4) the material of the insert

should have an intermediate value of the absorption coefficient of the laser radiation. The most suitable inserts for welding chromium–nickel steels with titanium alloys are assumed to be Cu and Ni or their alloys, and Ag and its alloys with Cu and Zn.

For welding dissimilar materials, it is preferable to use highly concentrated energy sources, such as electron beams and lasers, since in this case there are minimum structural changes in the heat-affected zones and narrow joints are formed with high penetration depth [2, 3]. In recent years, numerous works have been devoted to the effect of laser and electron-beam welding on the structural state and strength of joints between nickel–chromium steel and titanium alloys with various intermediate inserts [7–11]. Of special interest is the use of copper plates as the intermediate insert, since in this case welding joints are formed whose strength is close to that of the titanium alloy [6, 10, 12]. However, the data on the phase composition and structure of such joints are contradictory; moreover, there are no transmission-electron-microscopic data making it possible to detect the presence of reinforcing nanoparticles [13] and to investigate the substructure of the various zones of the welded joint.

This work is aimed at a comprehensive comparative analysis of the structural state of the laser-welded
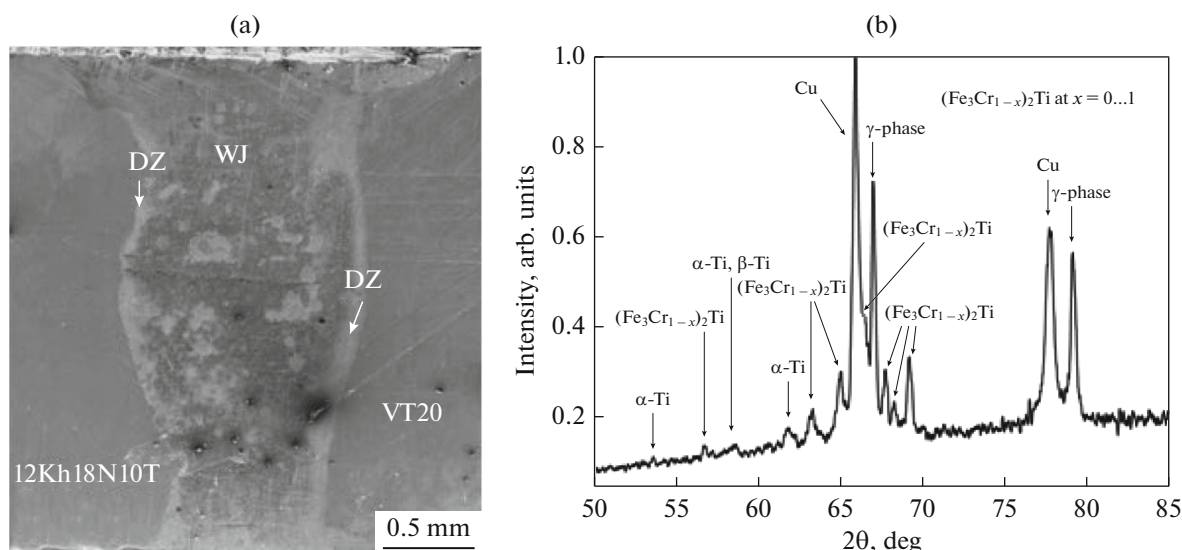
(a)

(b)

Fig. 1. (a) SEM image (secondary-electron mode) of the microstructure and (b) X-ray diffraction pattern of the welded joint.

joint between the 12Kh18N10T steel and the VT20 alloy with an intermediate copper insert.

EXPERIMENTAL

The laser welding of sheets of the 12Kh18N10T steel and VT20 titanium alloy with a thickness of 3 mm was carried out using a CO_2 laser with a radiation power of 2.2 kW and at a welding rate of 1.0 m/min with a 2-mm depth of the focus at the Khristianovich Institute of Theoretical and Applied Mechanics, Siberian Branch, Russian Academy of Sciences, under the guidance of Prof. A. M. Orishich. As the intermediate insert, we used a plate of copper of grade M1 with a thickness of 1 mm. The VT20 alloy had the following chemical composition (wt %): 5.9 Al; 1.4 V; 1.8 Zr; 0.9 Mo; and Ti for balance. The chemical composition of the steel was as follows (wt %): 0.08 C; 17.6 Cr; 9.5 Ni; 1.2 Mn; 0.4 Ti; 0.37 Si; 0.2 Mo; and Fe for balance. The laser beam was shifted toward the steel so that the center of the focal spot was directed to the boundary between the copper plate and the steel. As was previously found [12], this condition is the most favorable for forming the welded joint. To protect the surface of the welding pool and overheated near-weld zones, a mixture of carbon dioxide with air taken in a ratio of 1 : 7 was used; the gas pressure was 12 Torr.

The chemical composition of the welded materials was determined by the spectral analysis using a SPECTROMAXx device. The structural studies of the welded joint were carried out using a TESCAN VEGA II XMU scanning electron microscope and a JEM-200CX transmission electron microscope. The X-ray diffraction analysis was performed using a Shimadzu XRD 7000 diffractometer with a monochromatized $K\alpha$ radiation of the chromium anode in an

angular range of $2\theta = 50°{-}85°$. The energy-dispersive X-ray microanalysis was performed using a scanning electron microscope equipped with an OXFORD energy dispersive attachment.

The Vickers hardness and the microhardness were measured using a LEICA VMHT AUTO tester under a load of 9.8 and 0.49 N, respectively according to the requirements of the Russian Standards GOST 2999–75, GOST 9450–76, and GOST R ISO 6507-1–2007. The ultimate tensile strength was determined according to the GOST 6996–66 (ISO 4136-89) using an INSTRON 88011 tensile testing machine at a tensile rate of 1 mm/min. The samples for tests were cut across the welded joint so that the joint was located in the middle of the gage part of the sample.

RESULTS AND DISCUSSION

The width of the WJ formed by laser welding is 1.6 mm at half the sheet thickness and 2 mm in the upper part. Taking into account the copper-plate thickness (1 mm), it could be assumed that near-boundary layers of the materials to be joined with a thickness of 0.3 mm on each side participated in the formation of the welding pool. The intensive convective stirring of the melt in the welding pool led to a diffusion redistribution of atoms of molten titanium over the entire width of the welded joint up to the boundary with the steel, and a redistribution of iron, chromium, and nickel in the molten steel occurred over the entire width of the welded joint up to the titanium alloy. The material of the WJ represents a solid solution of the alloying elements in the crystal lattice of copper with intermetallic particles of various dimensions (Fig. 1a). The X-ray diffraction pattern of the WJ is seen (Fig. 1b) to contain α-Ti, β-Ti (very weak reflections),
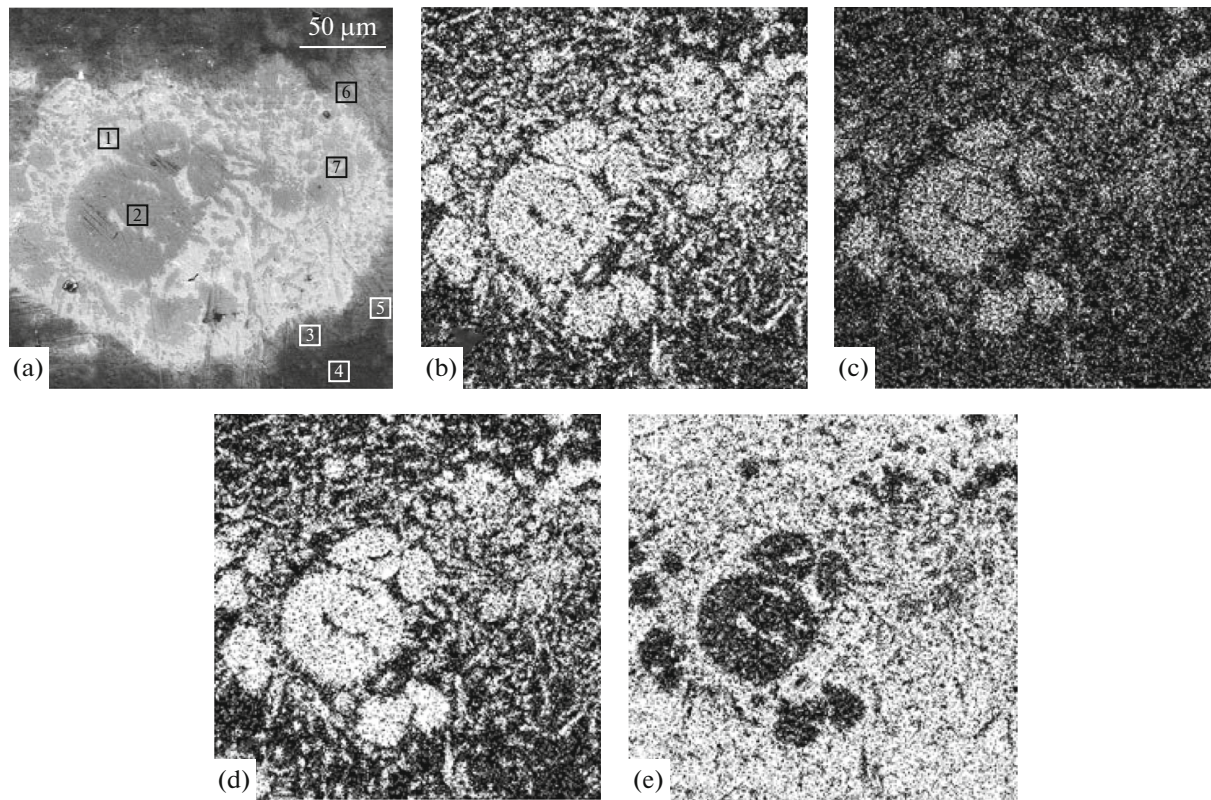
Fig. 2. (a) SEM image (secondary-electron mode) of coarse conglomerate; and energy-dispersive X-ray images in (b) Ti, (c) Cr, (d) Fe, and (e) Cu characteristic radiation of Ti.

γ-Fe, copper, chromium, and intermetallic compounds $(Fe_xCr_{(1-x)})_2Ti$, where x can vary from 0 to 1 (hereinafter, this intermetallic compound is designated as $(Fe,Cr)_2Ti$), and weak reflections of the Cu_3Ti intermetallic compound. The size of $(Fe,Cr)_2Ti$ and Cu_3Ti varies from 5 to 50 μm and from 1 to 10 μm, respectively. The presence of these intermetallic compounds is confirmed by the energy-dispersive X-ray microanalysis.

It is known that the crystallization processes upon laser welding occur at high cooling rates [2, 3]. The first phases to crystallize are several-micron $(Fe,Cr)_2Ti$ and Cu_3Ti intermetallic particles; then, a copper-based supersaturated solid solution crystallizes. The difference in the time of crystallization of these phases is a fraction of a second. Therefore, the solid solution is supersaturated with iron, titanium, and chromium, which had no time to form intermetallic compounds. In the regions with an insufficient convective stirring of the melt in the welding pool, the formation of coarse conglomerates with a size of up to 300 μm can occur, which look like coarse particles at small magnifications (Fig. 1a). The energy-dispersive X-ray microanalysis showed that each conglomerate consists of many fine intermetallic particles with different size, between which there is a solid solution based on copper (Fig. 2, Table 1).

The TEM studies showed that the copper solid solution contains homogeneously precipitated $(Fe,Cr)_2Ti$ particles with dimensions of 6–30 nm

Table 1. Chemical composition of a coarse conglomerate in regions indicated in Fig. 2a (wt %)

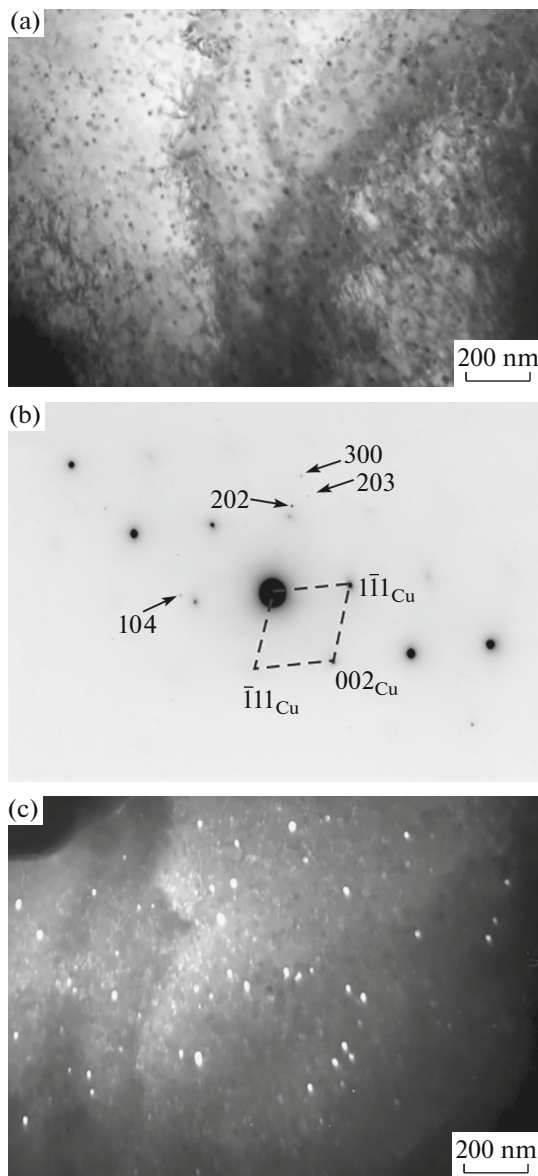| No.	Al	Si	Ti	V	Cr	Fe	Ni	Cu	Mo	Phase
1	0.6	0	2.3	0	0.5	1.8	1.4	93.4	0	Cu-based solid solution
2	0	0.3	12.7	0.7	16.9	52.5	4.7	12.9	0	$(Fe,Cr)_2Ti$
3	0.4	0	1.8	0	1.7	3.5	1.1	91.5	0	Cu + $(Fe,Cr)_2Ti$
4	0.3	0	0.8	0	0.6	1.7	0.9	95.1	0	Cu
5	0	0.2	12.6	0	5.7	25.5	2.2	53.8	0	Cu + $(Fe,Cr)_2Ti$
6	0	0.8	21.6	0.7	13.1	52.4	3.3	7.4	0.7	$(Fe,Cr)_2Ti$
7	0	0.5	17.9	0.6	8.6	37.8	2.5	31.4	0.7	

Fig. 3. Microstructure of the welded joint: (a) bright-field image; (b) electron-diffraction pattern (zone axis $[110]_{Cu}$, the arrows point the $(Fe,Cr)_2Ti$ reflections); and (c) dark-field image in reflections of $Cu + (Fe,Cr)_2Ti$.

Fig. 4. Microstructure of the welded joint: (a) bright-field image and electron diffraction pattern; and (b) dark-field image in the 115 Cu_4Ti reflection.

Fig. 5. Distribution of the microhardness over the width of the welded joint.

(Fig. 3) and Cu_4Ti particles with dimensions of 10–20 nm (Fig. 4). Obviously, such nanoscale intermetallic particles have time to form at high cooling rate from the supersaturated solid solution.

The mean hardness of the material of the WJ in the central part is 300 HV-1, while the microhardness varies from 250 to 700 HV-0.05 (Fig. 5). This is explained by the presence of both a copper-based solid solution with a low hardness (220–250 HV-0.05) and of intermetallic particles with a hardness of 550–700 HV-0.05. The mean hardness of the WJ closer to the steel region is slightly higher and is 380 HV-1.
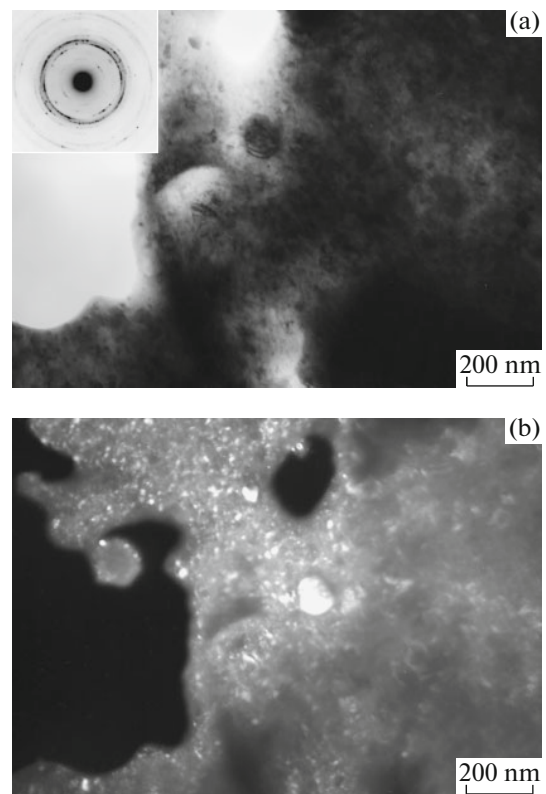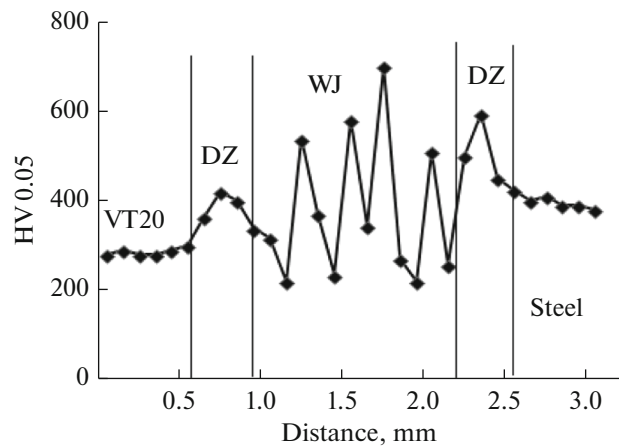
The hardness of the WJ near the titanium alloy is 320 HV-1. Considering that the hardness of the VT20 alloy and of the 12Kh18N10T steel is 250 and 350 HV-1, respectively, it can be assumed that the distribution of the hardness measured under a load of 9.8 N is almost uniform over the width of the WJ, excluding the diffusion zone (DZ) at the boundary with steel (594 HV-1), where martensite was found (Fig. 6).
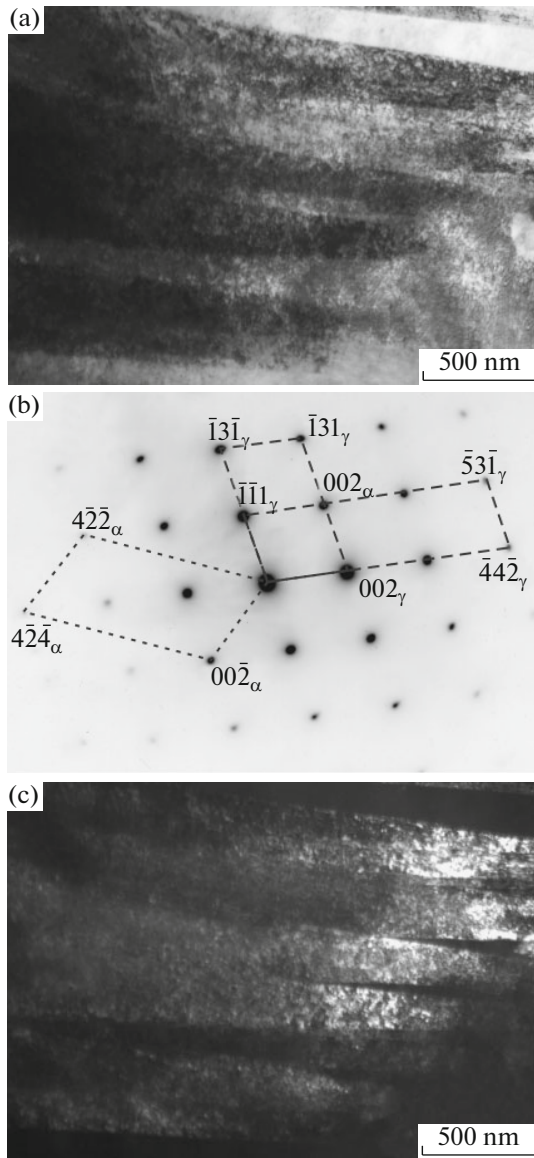
Fig. 6. Structure of the steel near the welded joint: (a) bright-field image; (b) electron diffraction pattern (zone axes $[120]_\alpha$, $[134]_\gamma$, and $[130]_\gamma$); and (c) dark-field image in the 002_α reflection.

Fig. 7. Distribution of elements over the width of the DZ at the boundary with (a) VT20 alloy and (b) steel: (—■—) Ti; (—▲—) Cr; (—×—) Fe; (—∗— Ni; (—●—) Cu.

The energy-dispersive X-ray microanalysis revealed that diffusion zones with widths of 0.2−0.4 mm are formed on both sides of the boundaries between the WJ and the materials to be joined (Fig. 1a). Figure 7 shows the distribution of elements over the width of these zones. The high copper content (30−40 wt %) in the DZ is explained by the presence of nanoscale Cu_4Ti particles homogeneously precipitated similar to that shown in Fig. 4 from the supersaturated solid solution upon cooling. The appearance of martensite after rapid cooling in the layer located close to the WJ of the steel layer is apparently caused by a change in
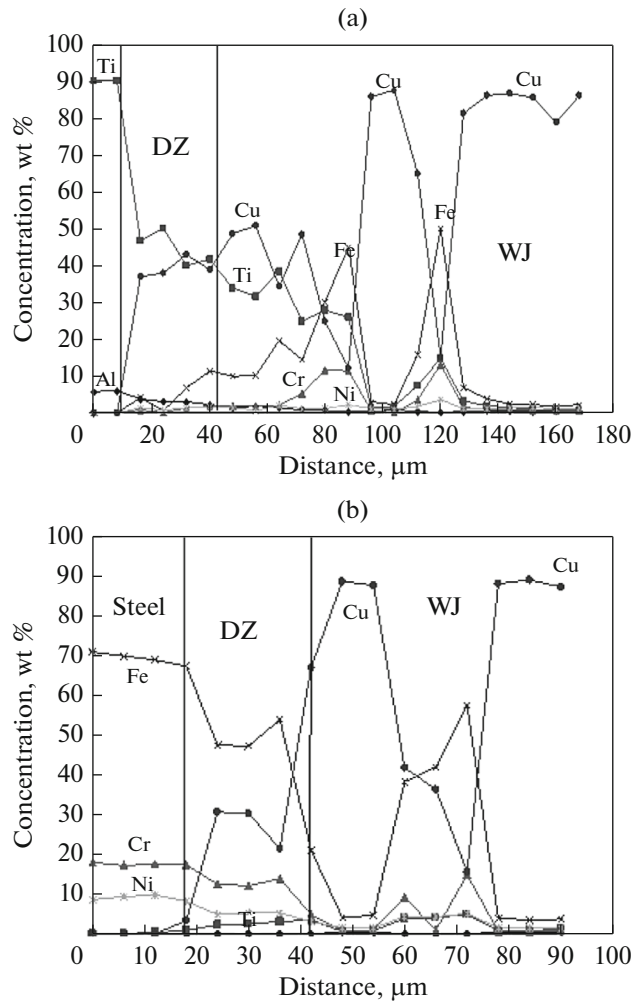
the steel chemical composition—austenite is supersaturated with titanium and copper (Fig. 7b).

The strength of the WJ of the tested samples was different: the values of the ultimate tensile strength were 266, 333, and 474 MPa. In all cases, the fracture occurred along the DZ at the boundary with the titanium alloy (Fig. 8a). The fracture surface is seen (Fig. 8b) to contain both regions of ductile fracture and cleavage regions characteristic of brittle fracture. According to the data of the energy-dispersive X-ray microanalysis, the regions of the ductile fracture correspond to the material of the WJ, since they mainly contain copper and intermetallic particles, around which the delamination takes place (Fig. 8c). The brittle fracture with numerous secondary cracks correspond to the DZ at the boundary between the WJ and the titanium alloy. Most likely, the material of the DZ at the boundary with the VT20 alloy tends to the brittle fracture since the alloying of this zone with copper, iron, chromium, and nickel (see Fig. 7a) increases the
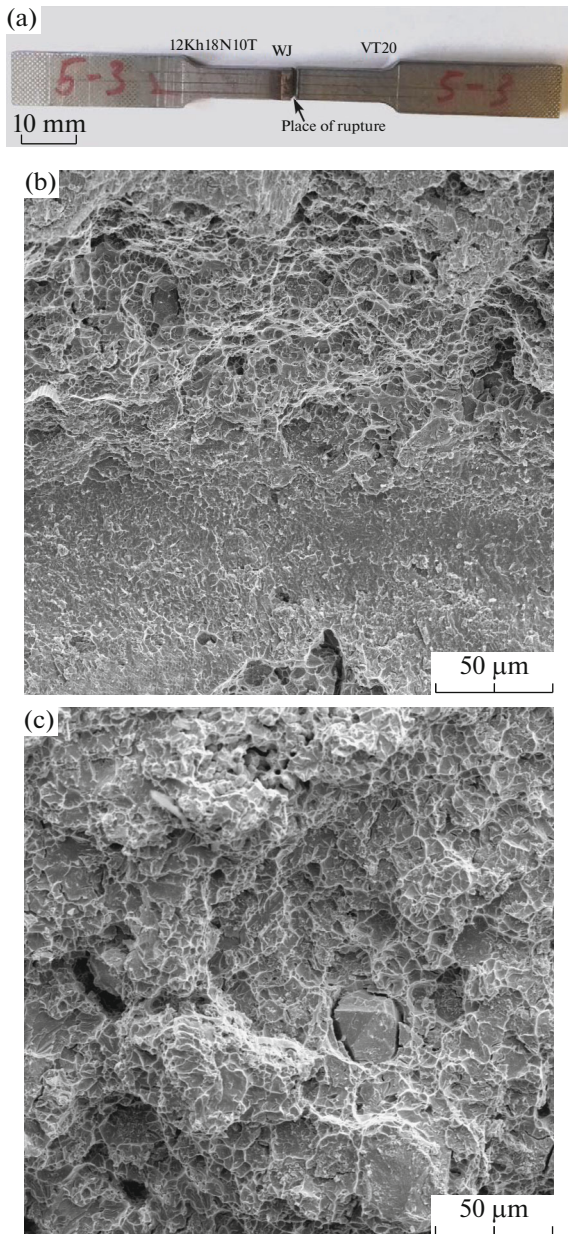
(a)

12Kh18N10T   WJ   VT20

10 mm   Place of rupture

(b)

50 μm

(c)

50 μm

Fig. 8. (a) Overall view of the sample after tensile test, (b) SEM image of the fracture surface with brittle and ductile fracture regions, and (c) SEM image of the fracture surface along the welded joint with a $(Fe,Cr)_2Ti$ particle indicated by arrow.

stability of the β phase, which transforms into martensite (α′ and α″ phases) at high cooling rates, which, as is known [15–17], leads to a substantial embrittlement of titanium alloys.

The differences in the values of the ultimate tensile strength are associated with the fact that the fracture captured different volumes of the WJ: in the sample with the minimum strength ($\sigma_u = 266$ MPa), the regions of brittle fracture prevail on the fracture surface along the DZ with the titanium alloy, and the

maximum $\sigma_u = 474$ MPa corresponds to the fracture with a greater fraction of the material of the WJ.

CONCLUSIONS

It has been found that the material of the welded joint between the 12Kh18N10T steel and the VT20 alloy with an intermediate copper insert represents a copper-based solid solution with intermetallic particles $(Fe,Cr)_2Ti$ with dimensions of 5–50 μm and Cu_3Ti with dimensions of 1–10 μm, which were the first to be formed in the course of crystallization of the melt in the welding pool. The microhardness of the intermetallic particles is 550–700 HV-0.05. The TEM studies showed that $(Fe,Cr)_2Ti$ and Cu_4Ti particles with dimensions of 10–30 nm precipitated uniformly in the copper-based solid solution upon cooling. The microhardness of the copper-based solid solution with nanoparticles of $(Fe,Cr)_2Ti$ and Cu_4Ti is 220–250 HV-0.05.

It has been shown that at the boundaries between the material of the laser-welded joint and the components to be joined, diffusion zones are formed containing up to 30–40 wt % copper with widths of 0.2–0.4 mm on each side of the joint. These diffusion zones are supersaturated solid solutions based on iron or titanium with nanoparticles of Cu_4Ti uniformly precipitated upon cooling.

The hardness measured under a load of 9.8 N varies smoothly over the width of the welded joint from 250 HV-1 for the VT20 alloy to 350 HV-1 for the 12Kh18N10T steel. In the diffusion zone at the boundary with the steel, the hardness is somewhat higher and is 594 HV-1, which is due to the formation of martensite on rapid cooling of austenite enriched with titanium and copper.

The fracture of the samples upon tension begins in the diffusion zone at the boundary with the VT20 titanium alloy and develops along the material of the welding joint. The differences in the ultimate tensile strengths of the samples are explained by the different amount of the material of the welded joint captured upon fracture: in the fracture surface of the sample with $\sigma_u = 266$ MPa, regions of brittle fracture prevail in the material of the titanium alloy; in the fracture surface of the sample with $\sigma_u = 474$ MPa, the dimple fracture along the material of the welded joint prevails.

REFERENCES

1. S. Katayama, *Handbook on Laser Welding*, Ed. by N. L. Istomina (TEKhNOSFERA, Moscow, 2015) [in Russian].

2. N. N. Rykalin, A. A. Uglov, I. V. Zuev, and A. N. Kokora, *Laser and Electron Beam Treatment of Materials* (Mashinostroenie, Moscow, 1985) [in Russian].

3. A. G. Grigor'yants and I. N. Shiganov, *Laser Equipment and Technology. In 7 books. Book 5. Laser Welding of Metals: Textbook for Universities* (Vysshaya shkola, Moscow, 1988) [in Russian].

4. V. E. Zinov'ev, *Thermophysical Properties of Metals at High Temperatures* (Metallurgiya, Moscow, 1989) [in Russian].

5. S. Kundu, S. Sam, and S. Chatterjee, "Interface microstructure and strength properties of Ti−6Al−4V and microduplex stainless steel diffusion bounded joints," Mater. Des. **32**, 2997−3003 (2011).

6. A. N. Cherepanov, Yu. V. Afonin, and A. M. Orishich, "Laser welding of steel with titanium alloy using intermediate inserts and nanopowder inoculators," Tyazheloe Mashinostroenie, No. **8**, 24−26 (2009).

7. S. Chen, M. Zhang, J. Huang, C. Cui, H. Zhang, and X. Zhao, "Microstructures and mechanical property of laser butt welding of titanium alloy to stainless steel," Mater. Des. **53**, 504−511 (2014).

8. I. Tomashchuk, P. Sallamand, H. Andrzejewski, and D. Grevey, "The formation of intermetallics in dissimilar Ti6Al4V/copper/AISI 316 L electron beam and Nd:YAG laser joints," Intermetallics **19**, 1466−1473 (2011).

9. I. Mitelea, C. Groza, and C. Craciunescu, "Copper interlayer contribution on Nd:YAG laser welding of dissimilar Ti−6Al−4V alloy with X5CrNi18-10 steel," J. Mater. Eng. Perform. **22**, 2219−2223 (2013).

10. A. N. Cherepanov, A. M. Orishich, N. B. Pugacheva, and V. P. Shapeev, "Investigation of the structure and properties of titanium-stainless steel permanent joints obtained by laser welding with the use of intermediate inserts and nanopowders," Thermophys. Aeromech. **22**, 135−142 (2015).

11. N. B. Pugacheva, M. V. Myasnikova, and N. S. Michurov, "Simulation of the elastic deformation of laser-welded joints of an austenitic corrosion-resistant steel and a titanium alloy," Phys. Met. Metallogr. **117**, 195−203 (2016).

12. V. I. Isaev, A. N. Cherepanov, and V. P. Shapeev, "Numerical study of heat modes of laser welding of dissimilar metals with an intermediate insert," Int. J. Heat Mass Transfer **99**, 711−720 (2016).

13. N. B. Pugacheva, N. P. Antenorova, and E. I. Senaeva, "Study of the structure and properties of laser-welded joints of the Al−Mg−Li alloy," Phys. Met. Metallogr. **116**, 1259−1269 (2015).

14. N. S. Michurov, I. A. Veretennikova, N. B. Pugacheva, and E. O. Smirnova, "The structural state and geometric representation of a laser-welded joint between a corrosion-resistant steel and a titanium alloy with a copper insert," AIP Conf. Proc. **1909**, 020137 (2017). https://doi.org/10.1063/1.5013818

15. S. P. Belov, M. Ya. Brun, and S. G. Glazunov, *Metal Science of Titanium and Its Alloys* (Metallurgiya, Moscow, 1992) [in Russian].

16. N. V. Kazantseva, I. V. Ezhov, N. I. Vinogradova, M. V. Il'inykh, A. S. Fefelov, D. I. Davydov, O. A. Oleneva and M. S. Karabanalov, "Effect of built geometry on the microstructure and strength characteristics of the Ti−6Al−4V alloy prepared by the selective laser melting," Phys. Met. Metallogr. **119**, 1079−1086 (2018).

17. A. G. Illarionov, S. V. Grib, S. M. Illarionova, and A. A. Popov, "Relationship between structure, phase composition, and physicomechanical properties in quenched Ti−Nb alloys," Phys. Met. Metallogr. **120**, 150−156 (2019).

Translated by O. Golosova